Volume 17
Number 19
21 May 2025
Pages 11765-12520

Nanoscale

rsc.li/nanoscale

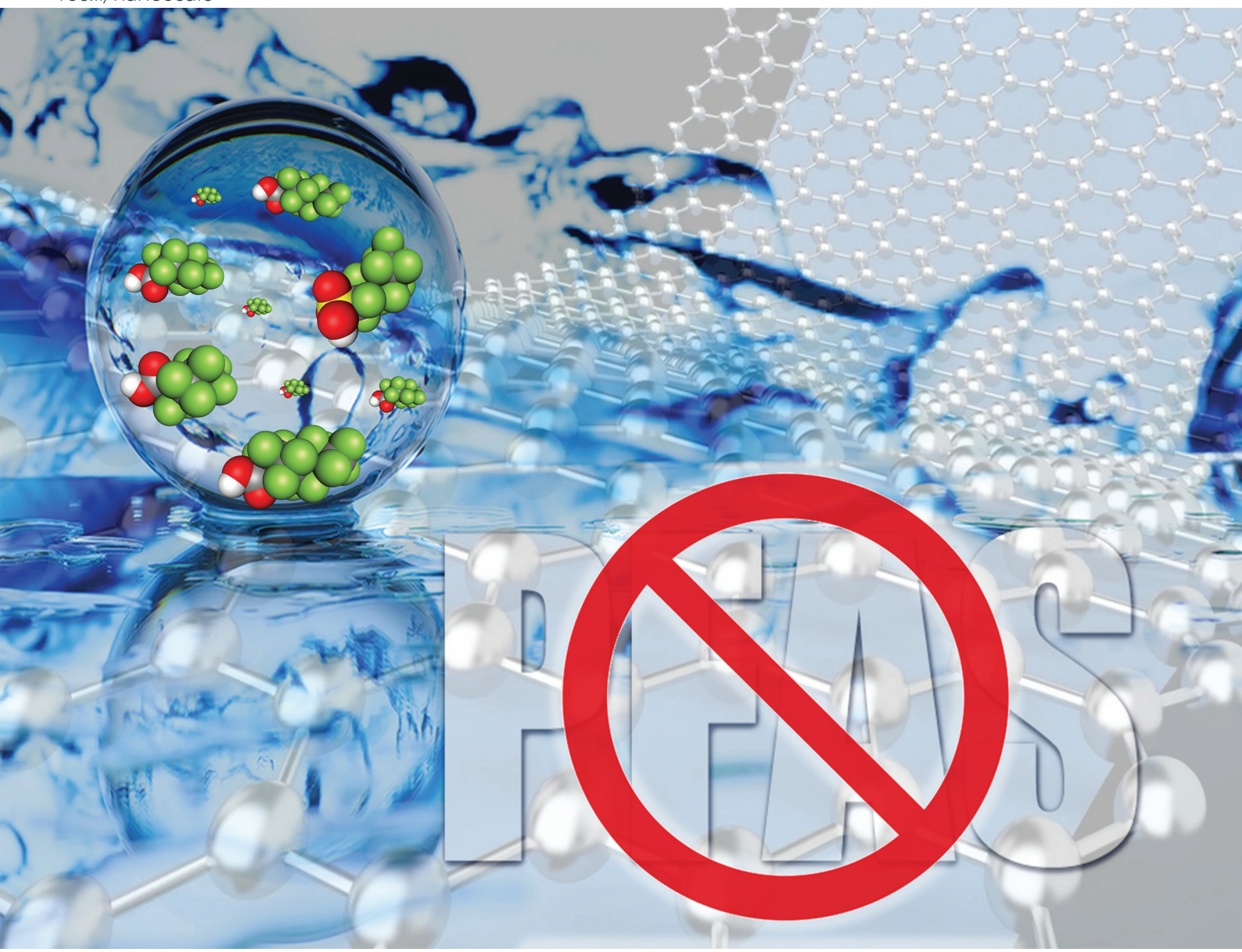

ISSN 2040-3372

ROYAL SOCIETY OF CHEMISTRY

PAPER

Matteo Calvaresi, Manuela Melucci *et al.*

Tailoring graphene oxide nanosheets by alkyl amine grafting for enhanced adsorption of PFASs in drinking water: a combined theoretical and experimental study

NCNST

Nanoscale

PAPER

View Article Online
View Journal | View Issue

Cite this: *Nanoscale*, 2025, **17**, 12124

Tailoring graphene oxide nanosheets by alkyl amine grafting for enhanced adsorption of PFASs in drinking water: a combined theoretical and experimental study†

Andrea Trifoglio,[a,b] Sebastiano Mantovani,[a] Sara Khaliha,[a] Alessandro Kovtun,[a] Tainah Dorina Marforio, [b,c] Matteo Calvaresi *[b,c] and Manuela Melucci *[a]

Per- and polyfluoroalkyl substances (PFASs) are a class of persistent organic pollutants present in natural water showing environmental and health risks. Most of the currently available purification technologies fail in the removal of short and medium perfluoroalkyl chain length PFASs. Here, we report the design and synthesis of graphene oxide (GO) modified with different alkyl- and alkylamine pendants including *N*,*N*-dimethylethylenediamine (GO-DMEN) and investigate the relationships between the chemical structure of the alkyl pendant and the adsorption of PFAS molecules of different sizes and end group type. GO-DMEN shows higher removal (up to 98%) after 15 minutes toward medium and long chain PFASs, such as perfluorohexanoic acid (PFHxA) and perfluoroheptanoic acid (PFHpA), poorly removed by unmodified GO. Molecular modeling shows that van der Waals interactions are the driving forces for the adsorption. Indeed, the quaternarization of the amine moieties, with the consequent creation of positive charges on graphene nanosheet surfaces, does not enhance the adsorption capacity. The key role of the modification with an amine ended chain such as DMEN was demonstrated by comparing GO-DMEN adsorption properties to those of an octyl chain modified GO (GO-OcA) characterized by poorer binding energy contribution as a result of the flattening of the hydrophobic octyl chain on GO nanosheets (self-poisoning). This work contributes to a deeper understanding of the chemical interactions driving the adsorption of amphiphilic and charged PFAS molecules.

Received 4th February 2025,
Accepted 23rd March 2025

DOI: 10.1039/d5nr00502g

rsc.li/nanoscale

Introduction

Per- and polyfluoroalkyl substances (PFASs), known as "forever chemicals", have garnered worldwide attention due to their extensive utilization in daily commodities, their persistence within the ecosystem and human physiology, and their confirmed adverse effects on both ecological systems and human health.[1,2] PFASs have found widespread applications in several industrial products spanning from food packaging, non-stick cookware, coatings, waterproof clothing, and beauty products to firefighting foams.[3] Moreover, the disposal of such products or their by-products results in the dissemination of PFASs, leading to their accumulation across various environmental compartments, including water sources.[4–6] The strength of C–F bonds (485 kJ mol^{-1})[7] and the extremely low concentrations of PFASs in water (from a few to tens of thousands of ng L^{-1})[8] represent notable challenges for their removal through conventional water treatment methodologies.

PFAS removal from drinking water has become a relevant issue, increasing academic and industrial research.[9,10] To remove PFASs from aqueous environments, plenty of water treatment technologies have been evaluated. Among the possible solutions, adsorption remains the most used treatment method. Granular activated carbon (GAC) and ion-exchange resins (IERs) are the most exploited sorbents for PFAS mitigation.

GAC adsorption is currently the benchmark method for PFAS removal for both small scale water treatment, like point of use (POU) purification, and large scale wastewater/drinking water purification.[11,12] It has been demonstrated that the adsorption is mainly driven by hydrophobic interactions between carbon surface groups and PFAS molecules.[13] Hence,

[a]*Institute for Organic Synthesis and Photoreactivity (ISOF), National Council of Italy (CNR), Bologna, Italy. E-mail: manuela.melucci@cnr.it*
[b]*Alma Mater Studiorum – University of Bologna, Department of Chemistry 'G. Ciamician', Bologna, Italy. E-mail: matteo.calvaresi3@unibo.it*
[c]*IRCCS Azienda Ospedaliero – Universitaria di Bologna, Bologna, Italy*

†Electronic supplementary information (ESI) available: X-Ray photoelectron spectroscopy (XPS) and attenuated total reflectance Fourier transform infrared (ATR-FTIR) spectroscopy, ultra performance liquid chromatography-tandem mass spectrometry (UPLC-MS/MS), and molecular dynamic simulation results. See DOI: https://doi.org/10.1039/d5nr00502g

the efficacy of GAC is related to the carbon chain length of PFAS,[14] with the short and medium chain PFASs, characterized by elevated aqueous solubility, poorly adsorbed by GAC due to the lower hydrophobic interaction extent.[15]

Another sorbent to address PFAS removal is represented by ion-exchange resins which have proven to overcome the performance of GAC.[16] Polystyrene resins with quaternary ammonium functional groups (punctual positive charges) showed high adsorption performances toward most PFASs.[17–19] Adsorption performances up to 2390 mg of perfluorooctanesulfonic acid (PFOS, $(CF)_8$) per gram of sorbent have been reported for Purolite acrylate-based resins.[17] For such materials, the positively charged surface interacts electrostatically with the negatively charged pollutant while the hydrophobicity of the resin's backbone plays a crucial role in the adsorption of PFASs.

Membrane based technologies such as microfiltration (MF), reverse osmosis (RO) and nanofiltration (NF) have also been investigated.[20,21] For such technologies, PFAS rejection relies on membrane porosity and/or membrane surface charge[22,23] with 99% medium-long chain PFAS ($(CF)_{>5}$) rejection for both NF and RO in lab scale experiments at high feed concentrations (0.5–1600 ppm).[24] However, membrane fouling caused by PFAS adsorption cannot be avoided with a subsequent negative influence on rejection and permeation[21] and challenges are related to the disposal of the retentates. Recently, Fang *et al.* reported the synthesis of polyacrylonitrile membranes grafted with tertiary amino groups and their quaternarized form.[25] Quaternarization of the amine group results in the elevation of the isoelectric point leading to the formation of positive charges that enhance the electrostatic attraction toward PFASs.

In this scenario, nanomaterials are attracting increasing interest for the possibility of exploiting their high surface area and tunable surface chemistry. Among them, carbon nanotubes (CNTs) gained attention due to their higher adsorption capability, with removal efficiency toward PFOSs up to 1651 mg g^{-1}.[26,27] CNTs rely on hydrophobicity as the dominant interaction for PFAS adsorption. It follows that CNTs are able to remove up to 95% of perfluorooctanoic acid (PFOA, $(CF)_7$) but only 7.5% of the more hydrophilic perfluorobutanoic acid (PFBA, $(CF)_3$).[28] Moreover, PFASs are anionic in aqueous solution and the exposed surface of CNTs is negatively charged, thus limiting the adsorption capacity due to repulsive electrostatic interactions with PFAS molecules that are negatively charged.[28]

More recently, the efficacy of graphene oxide (GO) and its derivatives on the removal of emerging contaminants from drinking water has been reported.[29–32] The most crucial features of GO are its large surface area and tunable surface chemical groups[33] that can promote the adsorption of pollutants *via* H-bonds, ionic interactions and metal-ion complexation.[29]

Previously, GO nanosheets have been proposed for PFAS adsorption through a two-step procedure based on batch adsorption and tandem microfiltration.[34] Moreover, we demonstrated that GO integration in polysulfone hollow fiber membranes (now commercially available as Graphisulfone®)[35] may promote synergic adsorption and ultrafiltration with removal capability toward different PFASs, mainly long chain molecules.[36]

Theoretical modeling demonstrated that the adsorption derives from multiple interactions, including hydrophobic, electrostatic and van der Waals (vdW) interactions.[37] The removal of short and medium chain PFASs on GO is lower when compared to longer chain PFASs. The electrostatic interaction between PFASs and GO is always unfavorable due to the repulsion between negatively charged PFASs and negatively charged GO nanosheets.[29] When the vdW interaction is able to fully overcome the electrostatic term, such as in the case of longer chain PFASs, they are efficiently adsorbed by GO.[38]

To enhance the binding energy between PFAS molecules and GO nanosheets we envision the possibility of tuning the surface chemistry of GO nanosheets by covalent modification. To this end, we demonstrated that β-cyclodextrin modified GO nanosheets, obtained by GO epoxide ring opening reaction, promote highly efficient removal of PFBA thanks to a synergic effect of β-CD complexation of PFBA and alkyl linker promoted entrapping of PFBA between the GO nanosheet and the cavity of β-CD in a sandwich-like structure.[38–40]

Here, we designed and synthesized a rational family of alkyl chain modified GO bearing polar, charged or hydrophobic chains (Fig. 1). Specifically, we synthesized *N*,*N*-dimethylethylenediamine-modified graphene oxide (GO-DMEN) including its quaternarized form GO-QDMEN, bearing a positively charged ammonium end-group and octylamine modified GO (GO-OcA). Through a combined experimental and theoretical study, here we investigate the interactions involved in the PFAS adsorption process from amino-modified GO to ultimately unravel the parameters the adsorption mechanism of PFASs on modified GO depends on.

Results and discussion

Synthesis and characterization

The synthesis of GO derivatives was achieved using an epoxide ring opening reaction starting from the commercially available *N*,*N*-dimethylethylenediamine (DMEN). Three different stoichiometric ratios of GO : DMEN (1 : 1 (A), 1 : 3 (B) and 1 : 15 (C), respectively) were selected to evaluate the effect of amine loading on GO nanosheets on the adsorption properties.

GO-DMEN was quaternarized by nucleophilic substitution by using BuI as an electrophile (Scheme 1) to generate positive charges on GO-DMEN. Finally, GO-OcA was also synthesized, using octylamine (OcA) for the modification of GO, to investigate the behavior of a pure alkyl chain, that does not present the terminal tertiary nitrogen of DMEN.

The synthesized materials were purified by reiterated washing and centrifugation steps until no amine was found in the washing supernatant. The lyophilized materials were characterized by X-ray photoelectron spectroscopy (XPS) and attenuated total reflectance infrared (ATR-IR) spectroscopy, and their properties are compared to those of pristine GO. The

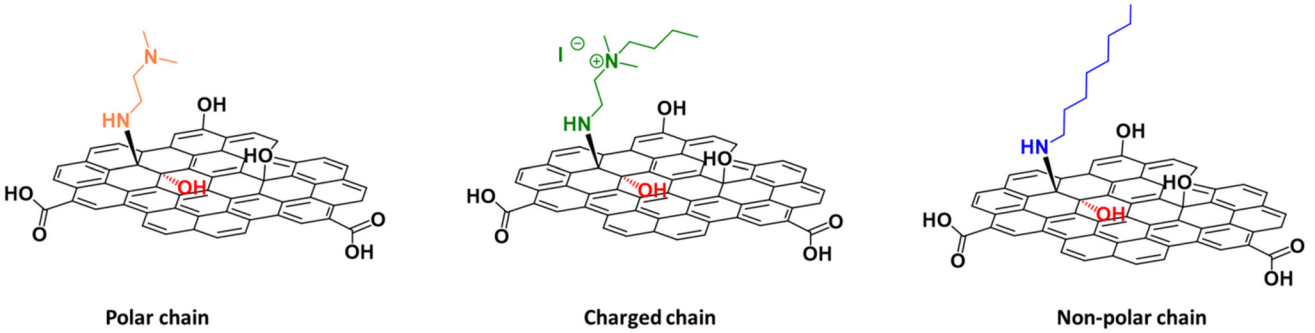

Fig. 1 Targeted modified GO studied in this work to tailor the interaction between PFAS molecules in water and functionalized GO with polar, charged and non-polar chains.

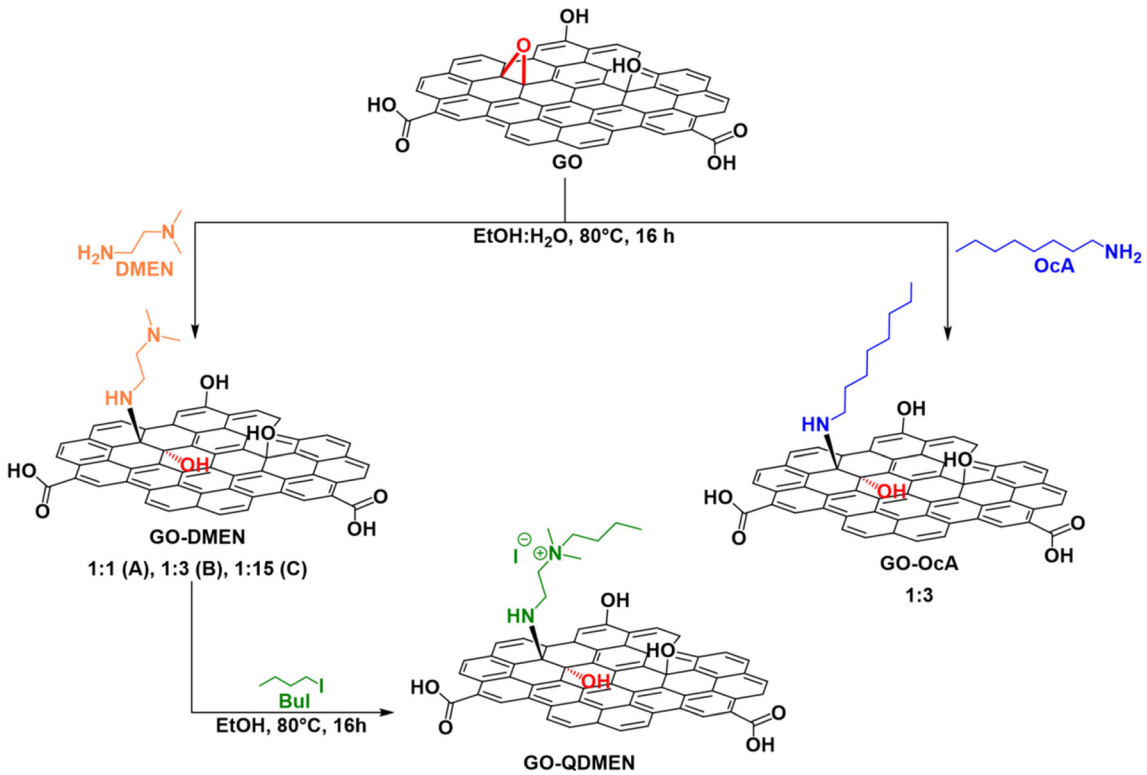

Scheme 1 Synthetic route to GO-DMEN, GO-QDMEN and the control material GO-OcA.

XPS survey spectra, N_{1s} high-resolution spectra and IR characterization of the materials are reported in the ESI.† The atomic compositions of GO and each modified GO are reported in Table 1. Since C and O are both present in the starting material, the most significant information on the composition was obtained from the N_{1s} and I_{3d} signals. The increase of the nitrogen content in GO-DMEN-A, GO-DMEN-B, and GO-DMEN-C with respect to GO (Table 1) was exploited for loading estimation (details in the ESI†). As shown by Table 1, the estimated loading was in the range of 12 and 19% for all the GO-DMEN products while for GO-OcA a higher value was found (33%). This high value for OcA can be ascribed to the strong hydrophobicity of the long octyl chain.

Table 1 XPS data showing the atomic compositions of GO and modified GO

XPS data	C %	O %	N %	I %	Loading %
GO	72.3	27.7	0.8	—	—
GO-DMEN-A	81.6	14.4	4.0	—	12
GO-DMEN-B	79.1	16.3	4.6	—	14
GO-DMEN-C	82.3	11.6	6.3	—	19
GO-QDMEN	77.2	17.7	4.1	0.97	13
GO-OcA	79.4	17.4	3.7	—	33

The effective quaternarization of the terminal nitrogen was confirmed by the presence of I_{3d} signals. Pristine GO and GO-DMEN-B do not contain iodine, while after the reaction,

GO-QDMEN has an iodine content of 0.97%. Furthermore, the shape of the nitrogen peak changes, with the N 1s peak of GO-QDMEN presenting a higher amount of quaternized nitrogen (signal at 402.5 eV in Fig. S1d†) compared to GO-DMEN-B. After quaternarization, GO-QDMEN presents an increased amount of quaternary nitrogen that contributes up to 30% of the N 1s signal, which can be ascribed to the alkylation of the tertiary amine exposed by GO-DMEN nanosheets. This value is in good agreement with the amount of iodine, *i.e.* the counter ion of the alkylated tertiary amine (ammonium ion).

Adsorption of PFASs by modified GO

GO-DMEN-A, -B, and -C and GO-OcA were used as sorbents under batch conditions for a mixture of eight PFAS molecules, characterized by different chain length ($(CF)_3$–$(CF)_8$) and end group substitution (sulphonate and carboxylate, Fig. 2). The targeted initial concentration of the PFAS mixture (0.5 μg L^{-1} for each PFAS) was selected according to the environmentally relevant concentration generally found in drinking water sources (0.1–3 μg L^{-1}).[41]

The removal was estimated by UPLC-MS-MS (details of the method in the ESI†) after 15 minutes of contact time.

Effect of DMEN chain modification on PFAS removal

Fig. 3a shows the removal of each PFAS from tap water after 15 min using GO-DMEN-A, -B, and -C and using GO as a comparison.

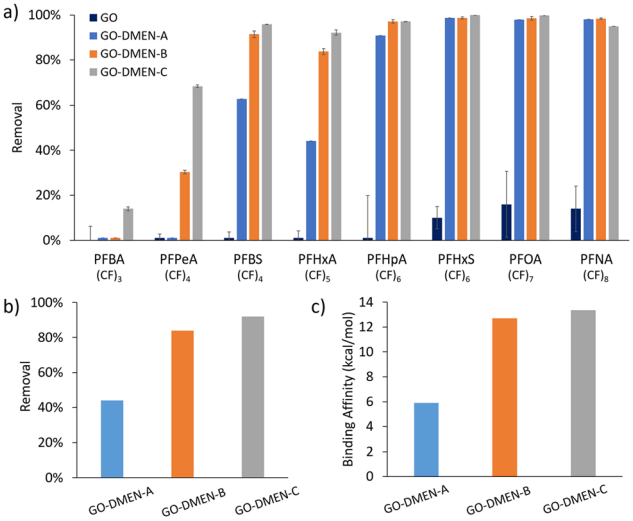

Fig. 3 (a) Removal of the PFAS mixture using GO-DMEN-A/B/C and GO. (b) Removal of PFHxA using GO-DMEN-A/B/C. (c) Calculated binding affinity ($\Delta E_{binding}$) of PFHxA for GO-DMEN-A/B/C. All energies are reported in kcal mol^{-1} and reported as absolute values. Details of removal calculations are given in the Experimental section.

GO-DMEN materials outperform GO in the removal of short and medium chain PFASs with removal up to 90% for long chain PFASs ($(CF)_{6–8}$) (*vs.* 20% of GO). On the other hand, GO shows negligible adsorption for medium chain PFASs ($(CF)_{4–5}$)

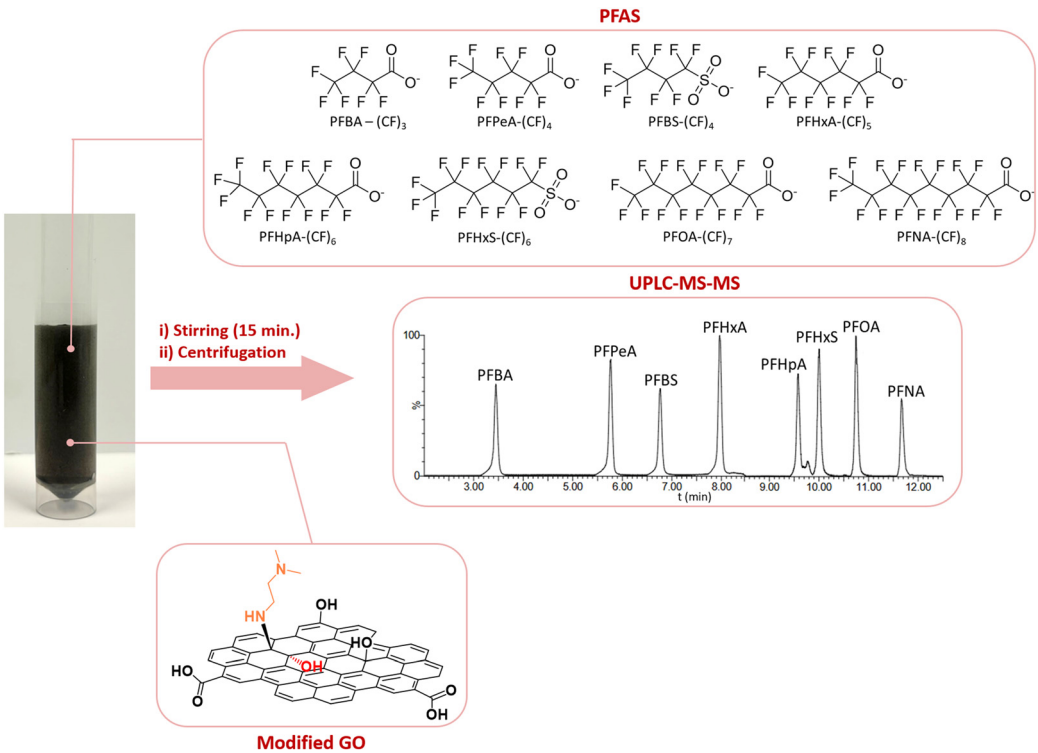

Fig. 2 The molecular structure of PFAS, a typical UPLC-MS-MS chromatogram and a sketch of the adsorption experiment set-up. A suspension of modified GO in ultrapure water was spiked with a mixture of short and medium chain PFASs ($(CF)_3$–$(CF)_8$), stirred for 15 minutes and centrifuged. The PFAS concentration of the supernatant was then analyzed using UPLC-MS-MS.

removed by GO-DMEN with values in the range 30–96%, with the highest shown by GO-DMEN-C (68–96%). Interestingly, PFPeA was removed by GO-DMEN-C with removal up to 68% *vs.* 30% observed for GO-DMEN-B. Regarding PFBA ($(CF)_3$), among the most persistent PFAS, it was poorly adsorbed only by GO-DMEN-C with a removal rate of 16%.

Although long chain PFASs are completely removed with no significant differences between the three synthesized materials, the selectivity toward medium chain PFASs is directly related to the increase in the DMEN amine loading. This is clearly shown by the adsorption of PFHxA, which is removed by GO-DMEN-A/B/C with the efficiency increasing from 44% to 84% to 92% GO-, respectively.

Molecular dynamics (MD) simulations were carried out to study the effect of different amine loadings on the removal ability of PFHxA. As shown in Table 2, GO-DMEN materials provide a favourable interaction with PFHxA, with binding energies ($\Delta E_{binding}$) of −5.9 (GO-DMEN-A), −12.7 (GO-DMEN-B) and −13.6 (GO-DMEN-C) kcal mol^{-1}. In agreement with the experimental results, the binding energy, and consequently the removal, increases at a higher amine loading (Fig. 3b and c).

Interestingly, stronger van der Waals interactions between PFHxA and grafted DMEN are the main forces governing the interaction between PFHxA and the modified graphene sheets. The increasing adsorption selectivity toward PFHxA can be ascribed to the formation of 3D recognition sites by the amine chains perpendicular to the basal plane of GO, increasing the shape complementarity between PFHxA and the sorbent surface.

Additionally, even to a minor extent, the non-polar solvation term (E_{SURF}), *i.e.* hydrophobic effect, contributes to the binding with PFHxA. On the opposite, the electrostatic term (E_{El}) seems to be detrimental to adsorption. This term accounts for: (i) the polar solvation term and (ii) the coulombic repulsion between the negatively charged carboxylate of PFHxA and the negatively charged GO. Even if hydrogen bonds or salt bridges can be formed between PFHxA and the amine moieties of GO-DMEN, the energy necessary to desolvate the two partners prevents such interactions. These findings support the fact that PFAS molecules are adsorbed only when the hydrophobic interactions (van der Waals plus hydrophobic effect) overcome electrostatic repulsion with GO materials. The results reported in Fig. 3b show that amine grafting increases the hydrophobic terms that are dependent on the amine loading.

PFHxA molecules show a preference for adsorption on regions of GO-DMEN, particularly around the DMEN pendants (Fig. S3†). The calculation of the distance distribution of F and O atoms of PFHxA relative to the graphene basal plane shows that the fluorine atoms of PFHxA have a marked tendency to adsorb on the basal plane of GO-DMEN, while the carboxylic oxygens of PFHxA protrude towards the water environment (Fig. S3†). The same results are observed relative to the DMEN chains, where DMEN tends to interact more closely with the fluorine atoms of PFHxA than with its carboxylates, confirming that hydrophobic interactions are favoured over hydrogen bonds/electrostatic interactions (Fig. S3†).

Table 2 Computed PFHxA binding affinity and its contributions *i.e.*, van der Waals (vdW), electrostatic (E_{El}) and non-polar solvation (E_{SURF}) for GO-DMEN-A/B/C. All energies are reported in kcal mol^{-1}

@PFHxA	Binding affinity	vdW	E_{El}	E_{SURF}
GO-DMEN-A	−5.9	−7.6	2.6	−0.8
GO-DMEN-B	−12.7	−14.2	3.0	−1.5
GO-DMEN-C	−13.6	−15.8	4.2	−2.0

Effect of charged DMEN chain modification on PFAS removal

The effect of electrostatic interactions on the PFAS removal ability of the GO-DMEN materials was investigated by synthesizing and studying the behaviour of a positively charged GO-DMEN obtained by the quaternarization reaction of GO-DMEN-B through its reaction with butyl iodide (Scheme 1). Fig. 4 shows the comparison of the removal of GO-DMEN-B and GO-QDMEN from the PFAS mixture ($(CF)_3$–$(CF)_8$) after 15 minutes of contact. Interestingly, the quaternarization of amine pendants does not affect significantly the removal of medium and long chain PFASs. Indeed, GO-QDMEN performances are in good accordance with those of GO-DMEN for all the medium and long chain PFASs ($(CF)_{4–8}$) with removal over 80%. For shorter PFASs after quaternarization, a poor improvement is observed, with GO-QDMEN adsorbing PFPeA with a removal rate of 46% *vs.* 30% observed for GO-DMEN. In the case of PFBA a similar trend was observed, with GO-DMEN showing negligible adsorption while a removal rate of 11% for GO-QDMEN. These results correlate well with the MD calculations demonstrating that electrostatic interactions do not play a crucial role in the adsorption (Fig. 5). Consequently, the increase of net positive charges on the GO surface does not affect the material's removal performance. van der Waals interactions remain the driving force for adsorption also for quaternarized materials, where the electrostatic interactions are even more unfavorable than in the case of GO-DMEN (Table 3).

Indeed, the energetic cost of the desolvation is larger than the potential Coulomb attraction among positively charged ammonium groups and the carboxylates of PFAS.

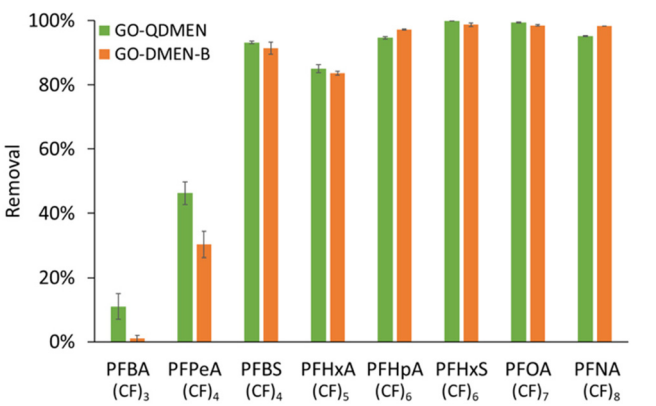

Fig. 4 Removal of the PFAS mixture using GO-DMEN-B and GO-QDMEN.

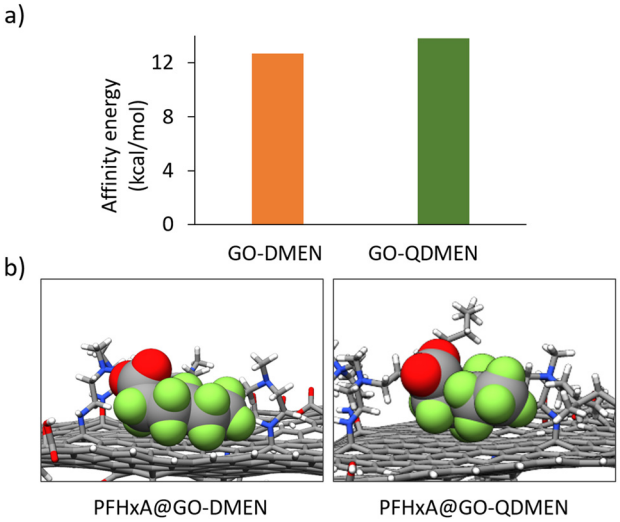

Fig. 5 (a) Calculated PFHxA binding affinity ($\Delta E_{binding}$) for GO-DMEN-B and GO-QDMEN. All energies are reported in kcal mol^{-1}. (b) Representative snapshots from MD simulations of PFHxA adsorbed on GO-DMEN and GO-QDMEN.

Table 3 Computed PFHxA binding affinity and its contributions *i.e.*, van der Waals (vdW), electrostatic (E_{El}) and non-polar solvation (E_{SURF}) for GO-DMEN and GO-QDMEN. All energies are reported in kcal mol^{-1} and reported as absolute values

@PFHxA	Binding affinity	vdW	E_{El}	E_{SURF}
GO-DMEN-B	−12.7	−14.2	3.0	−1.5
GO-QDMEN	−13.8	−17.0	5.3	−2.1

Effect of non polar octyl chain modification on PFAS removal

The effect of alkyl pendant functionalization of GO on the removal of the PFAS mixture was investigated by synthesizing and studying the adsorption properties of a GO functionalized with octylamine (OcA).

After GO grafting, OcA can expose the aliphatic chain to the surrounding environment allowing for the evaluation of the role of hydrophobic interactions between the OcA aliphatic moiety and PFASs during PFAS adsorption on modified GO nanosheets. Fig. 6 shows the comparison of the removal of PFASs by GO-OcA to that of GO-DMEN that presents the same oxidation level, but exposes the tertiary amine group to the solvent. The results suggest that the alkyl chain functionalization is not correlated with an increased removal. In fact, as shown in Fig. 6, GO-OcA does not remove medium-short chain PFASs as efficiently as GO-DMEN.

GO-OcA removal selectivity is negligible for short and medium chain PFASs ($(CF)_{3-5}$) and becomes more relevant for longer chain PFASs ($(CF)_{6-8}$), with a selectivity trend comparable to that of reduced graphene oxide (rGO), with the maximum removal observed for PFNA ($(CF)_8$, 83%). MD simulations (Fig. 7a and b) showed that the hydrophobic alkyl chains of OcA are adsorbed on the graphene basal plane,

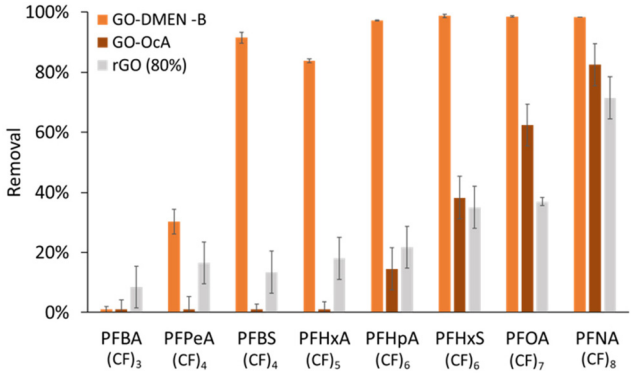

Fig. 6 Removal of the PFAS mixture from GO-DMEN-B compared to GO-OcA.

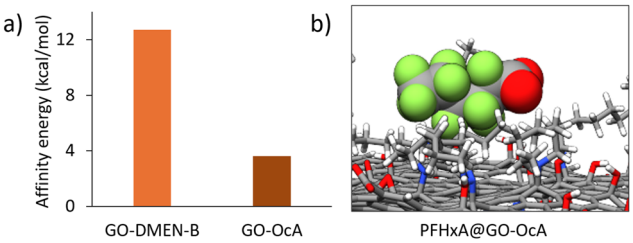

Fig. 7 (a) Calculated PFHxA binding affinity ($\Delta E_{binding}$) for GO-DMEN-B and GO-OcA. All energies are reported in kcal mol^{-1} and reported as absolute values. (b) Representative MD simulation snapshots of PFHxA on GO-OcA sheets.

coating the surface of the nanosheets. The hydrophobic OcA chains remain in vdW contact with the graphene basal plane, while the polar DMEN chain tends to protrude toward the solvent (Fig. S4†).

PFAS molecules ($(CF)_{6-8}$) can be adsorbed only at the formed sp_3 carbon carpet, strongly resembling the behaviour of the reduced graphene. The lower adsorption capability observed for GO-OcA further supports the crucial need for a terminal hydrophilic group in promoting the adsorption of PFASs. The free terminal tertiary amine present in the DMEN grafted on GO points toward the water environment, preventing the chain from lying on the GO basal plane and allowing for interaction with the water-dispersed pollutant. The hydrophobic methylene groups of DMEN enhance the interaction capability of GO with PFASs (Table 4).

Table 4 Computed PFHxA binding affinity and its contributions *i.e.*, van der Waals (vdW), electrostatic (E_{El}) and non-polar solvation (E_{SURF}) for GO-DMEN-B and GO-OcA. All energies are reported in kcal mol^{-1}

@PFHxA	Binding affinity	vdW	E_{El}	E_{SURF}
GO-DMEN-B	−12.7	−14.2	3.0	−1.5
GO-OcA	−3.6	−5.8	2.6	0.8

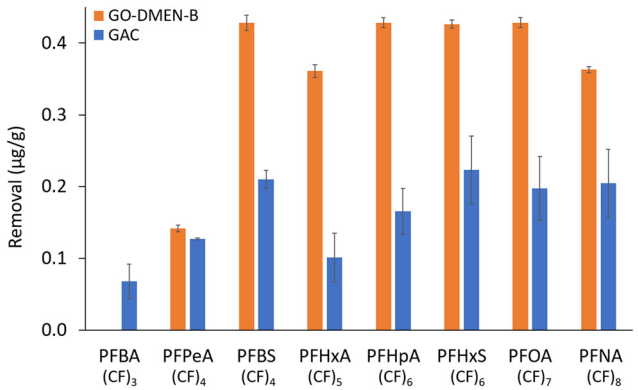

Fig. 8 Removal of the PFAS mixture from GO-DMEN-B compared to GAC. C_{IN} = 0.5 μg L^{-1}, and contact time = 15 min. Details of removal calculations are given in the Experimental section.

GO-DMEN *vs.* Granular Activated Carbon (GAC)

In order to evaluate the potential of the proposed materials for use in drinking water treatment, a comparison was made between the adsorption performance of GO-DMEN-B and that of GAC, which represents the current industrial benchmark for sorbent materials. Fig. 8 illustrates the comparison of the removal performances of GO-DMEN and GAC in terms of micrograms of PFASs removed per gram of sorbent.

The results demonstrate that GO-DMEN is more effective than GAC in the removal of PFASs. In particular, GAC captures the majority of the selected PFASs, with a maximum removal rate of 0.2 μg g^{-1}, while GO-DMEN reaches a removal rate of up to 0.4 μg g^{-1} after 15 minutes of contact time. The removal of PFPeA ($(CF)_4$) from GAC and GO-DMEN is comparable (0.13 μg g^{-1} *vs.* 0.14 μg g^{-1}, respectively). On the other hand, the shortest chain PFAS, *i.e.* PFBA, is only slightly captured by GAC (0.07 μg g^{-1}), while GO-DMEN shows no removal. The comparison between the benchmark sorbent and GO-DMEN is further highlighted when considering the total μg of PFASs removed per gram of material, which are 1.3 μg g^{-1} for GAC and 2.6 μg g^{-1} for GO-DMEN. Remarkably, the advantage of GO-DMEN relates not only to the highly efficient removal performances achieved but also to the faster kinetics reported, with high removal rates achieved after only 15 minutes of contact time. This is a crucial aspect of drinking water purification applications such as domestic point of use filters.

Conclusions

In conclusion, we have reported a new family of modified GO grafted with alkylamine pendants with different chemo-physical properties (hydrophobic, polar and charged chains), based on *N*,*N*-dimethylethylenediamine (GO-DMEN) and octylamine (GO-OcA). Through a combined theoretical and experimental approach, we investigated the relationships between the chemical structure of the alkyl amino pendant and the adsorption capability toward a mixture of PFASs with different chain lengths. Different amine loadings (ratio GO : DMEN 1 : 1, 1 : 3, 1 : 15) were considered and the PFAS removal selectivity of the synthesized materials was compared to that of pristine GO. All the GO-DMEN materials showed higher removal capability, than GO, with the highest performance achieved by GO-DMEN-C, *i.e.* that with the highest amine loading (19%). The role of the tertiary amine of DMEN was assessed by comparing the properties of GO-DMEN to those of GO-QDMEN, *i.e.* obtained by quaternarization of the tertiary DMEN amine and to those of GO-OcA obtained by reacting GO with octylamine, which has no terminal amine group. The results showed that (i) the presence of a positive charge on the GO-QDMEN nanosheets surface does not affect the adsorption selectivity, (ii) the absence of the terminal amine (GO-OcA) strongly reduces PFAS adsorption as a result of the flattening of the hydrophobic octyl chain on GO nanosheets and finally (iii) the adsorption properties of the GO-DMEN materials strongly depend on the DMEN loading. Remarkably, GO-DMEN-B outperforms GAC, the industrial sorbent benchmark, in the removal of the selected PFAS mixture at short contact time (15 minutes).

Overall, our results contribute to the understanding of the interactions that drive the adsorption between the graphene nanomaterial sorbent surface and PFAS molecules, paving the way to a specific design for advanced GO materials and technologies for water remediation.

Experimental section

Materials

Graphene oxide (GO) and reduced graphene oxide 80% (rGO, with approximately 80% C and 20% O) were purchased from Layer One (S-126/36) and used without further purification. Before using, GO was sonicated in ultrapure water to exfoliate the bulk material into a monolayer (>99%) with a lateral size of a few micrometers. GAC was purchased from CABOT Norit Spa (Ravenna, Italy, Norit GAC 830 AF, MB index min 240 mg g^{-1}, BET surface area >1000 m^2 g^{-1}) and used without further purification. PFAS standards were purchased from Agilent Technologies (Santa Clara, CA, US). The experiments on PFASs were carried out using polypropylene vials. All other chemicals were purchased from Sigma Aldrich or Thermo Fisher and used without any further purification.

Synthesis and purification of GO-DMEN-A, -B, and -C

To a suspension of GO (100 mg in 50 mL of EtOH : H_2O 1 : 1, 2 mg mL^{-1}) sonicated for 2 h at room temperature, and *N*,*N*-dimethylethylenediamine (DMEN) was added (100 mg for GO-DMEN-A, 300 mg for GO-DMEN-B and 1.5 g for GO-DMEN-C). The suspension was then refluxed (80 °C) under stirring overnight. After cooling to room temperature, the product was purified by reiterated washing with ethanol and Milli-Q water and centrifugation until the supernatant reached

pH neutrality. The so obtained materials were lyophilized and used for characterization and adsorption testing.

Synthesis and purification of GO-QDMEN

A suspension of GO-DMEN (5 mg mL^{-1}) in ethanol was sonicated for 2 h at room temperature, and then, BuI was added to the resulting solution to a final halide concentration of 20% v/v. The mixture was then refluxed (80 °C) overnight. After cooling to room temperature, the product was purified by reiterated washing with ethanol and ultrapure water and centrifugation until the supernatant became colorless. Finally, the resulting mixture was lyophilized to obtain GO-QDMEN.

Synthesis and purification of GO-OcA

To a suspension of GO (100 mg in 50 mL of EtOH : H_2O 1 : 1, 2 mg mL^{-1}) sonicated for 2 h at room temperature, 300 mg of octylamine (OcA) were added. The suspension was heated to reflux (80 °C) under stirring overnight. After cooling to room temperature, the product was purified by reiterated washing with ethanol and ultrapure water and centrifugation until the supernatant reached pH neutrality. The so obtained material (GO-OcA) was lyophilized, characterized and used for the adsorption experiments.

Characterization

ATR-FTIR spectra were recorded with an Agilent Cary 630 FTIR spectrophotometer, and the spectra are expressed as wavenumber (cm^{-1}).

High-resolution XPS was performed using a Phoibos 100 hemispherical energy analyser, using Mg Kα radiation ($h\omega$ = 1253.6 eV; X-ray power = 125 W) in the constant analyser energy (CAE) mode, with an analyser pass energy of 10 eV. The base pressure in the analysis chamber during analysis was 4.2×10^{-8} mbar. Spectra were fitted by using CasaXPS (**https://www.casaxps.com**) after Shirley background subtraction and all spectra were calibrated to the C 1s binding energy (285.0 eV). XPS samples were prepared by filtration of a water suspended solution of the dry powder of each material on cellulose, and then the films were dried and ground by fixing them on the sample holder with conductive carbon tape.

Adsorption experiments

25 mg of powder materials (GO, rGO, GO-DMEN-A, -B, and -C and GO-QDMEN) were sonicated in 25 mL of tap water for 2 h to exfoliate the bulk material into monolayer nanosheets. After sonication, a mixture containing eight PFASs (125 μL of a stock solution of 100 μg L^{-1} in MeOH) was added to the suspensions to obtain a final concentration of 0.5 μg L^{-1} in a final volume of 25 mL. For non-powder materials (*i.e.*, GAC), 25 mg of samples were directly added to 25 mL of tap water and 125 μL of PFAS mixture (100 μg L^{-1} in MeOH) to obtain a final concentration of 0.5 μg L^{-1}. Samples were then left under gentle agitation for 15 min and 1 h, and then each sample was centrifuged (10 min, 10 000 rpm) and analyzed using UPLC-MS/MS.

PFAS quantification

Samples containing PFASs were analyzed using UPLC-MS/MS (ACQUITY UPLC H-Class PLUS – XEVO TQS Micro mass detector, Waters). 1 mL samples were used as sources for automated injection. Chromatographic separation was performed on a reverse phase Waters Acquity UPLC CSH phenyl-hexyl (1.7 μm, 2.1 × 100 mm) column and Waters isolator column (2.1 × 50 mm). The column temperature was 34 °C, the flow rate was 0.3 mL min^{-1} and the injection volume was 40 μL, while the total run time was 8 min for PFBA and 21 min for the mixture of eight PFASs. The mobile phase consisted of a biphasic gradient, 2 mM NH_4OAc in a mixture of ultrapure water : methanol 95 : 5 as phase A, and 2 mM NH_4OAc in MeOH as phase B (further details are reported in ESI† section 3). % Removal was calculated as $(1 - (C_{final}/C_{blank})) \times 100$, while the removal in μg (adsorbed)/g (sorbent) was calculated as $[(C_{blank} - C_{final}) \times \text{volume}]$/g sorbent. The initial concentration of PFNA was slightly lower than those of the other PFAS molecules leading to a difference between PFOA and PFNA removal in μg/g slightly higher than the difference between the removal in %.

Molecular dynamics simulations

PFAS molecules were parameterized using the generalized AMBER force field (GAFF).[42] The atomic charges were obtained at the HF/6-31G(d) level, followed by restrained electrostatic potential (RESP) fitting. A GO sheet was modelled following the previously reported approach.[37] The different amine pendants were placed randomly on a graphene sheet to reproduce the experimental XPS data, affording GO-DMEN (at three different amine loading percentages), GO-QDMEN and GO-OcA. The GAFF force field was also used to describe the model systems. The complexes obtained by placing the PFAS molecules on GOs were solvated by TIP3P water molecules and the total charge was neutralized by adding counterions. Using Amber16,[43] the solvated complexes were minimized *via* a two-step protocol: (1) relaxation of only water molecules and (2) all the system let free to reach the minimum energy. Then, equilibration was carried out for 10 ns to heat the system from 0 to 298 K, employing an Andersen thermostat and periodic boundary conditions (PBCs).

Molecular dynamics (MD) simulations for 100 ns followed the equilibration step. The binding affinity of each PFAS towards the modified GOs was calculated using the molecular mechanics – generalized Born surface area (MM-GBSA) algorithm.

Author contributions

Andrea Trifoglio: methodology, investigation, reviewing and editing. Sebastiano Mantovani: methodology and investigation. Sara Khaliha: methodology and investigation. Alessandro Kovtun: reviewing and formal analysis. Tainah Dorina Marforio: investigation, methodology, and formal analysis. Matteo Calvaresi: methodology and investigation.

Manuela Melucci: conceptualization, validation, and writing – original draft.

Data availability

X-Ray photoelectron spectroscopy (XPS) and attenuated total reflectance Fourier transform infrared (ATR-FTIR) spectroscopy results are provided in the ESI.† This material is available free of charge *via* the Internet at **https://doi.org/10.1039/D5NR00502G**.

Conflicts of interest

There are no conflicts to declare.

Acknowledgements

The authors gratefully acknowledge the support of this work from the projects Life-Remembrance, ENV/IT/001001 Life Resource and Environment LIFE20 'Give plastic wastes from the production of hollow-fiber membranes a second life', and PNRR MUR project ECS_00000033_ECOSISTER. MM thanks M. Bergamini and M. Brunetti (Gruppo HERA Spa, Bologna, Italy) for providing samples of GAC used in their municipal plants. Tainah Dorina Marforio was supported by Fondazione Umberto Veronesi.

References

1 E. M. Sunderland, X. C. Hu, C. Dassuncao, A. K. Tokranov, C. C. Wagner and J. G. Allen, *J. Exposure Sci. Environ. Epidemiol.*, 2019, **29**, 131–147.
2 The U-turn on PFAS, *Nat. Water*, 2023, **1**, 993.
3 J. Gardiner, *Aust. J. Chem.*, 2015, **68**, 13–22.
4 M. Mastrantonio, E. Bai, R. Uccelli, V. Cordiano, A. Screpanti and P. Crosignani, *Eur. J. Public Health*, 2017, **28**, 180–185.
5 S. Castiglioni, S. Valsecchi, S. Polesello, M. Rusconi, M. Melis, M. Palmiotto, A. Manenti, E. Davoli and E. Zuccato, *J. Hazard. Mater.*, 2015, **282**, 51–60.
6 L. Giari, C. Guerranti, G. Perra, A. Cincinelli, A. Gavioli, M. Lanzoni and G. Castaldelli, *Sci. Total Environ.*, 2023, **876**, 162828.
7 S. Dolui, D. Kumar, S. Banerjee and B. Ameduri, *Acc. Mater. Res.*, 2021, **2**, 242–251.
8 S. Kurwadkar, J. Dane, S. R. Kanel, M. N. Nadagouda, R. W. Cawdrey, B. Ambade, G. C. Struckhoff and R. Wilkin, *Sci. Total Environ.*, 2022, **809**, 151003.
9 O. S. Arvaniti and A. S. Stasinakis, *Sci. Total Environ.*, 2015, **524–525**, 81–92.
10 M. G. Kibambe, M. N. B. Momba, A. P. Daso and M. A. A. Coetzee, *J. Environ. Manage.*, 2020, **255**, 109945.
11 R. Amen, A. Ibrahim, W. Shafqat and E. B. Hassan, *Sustainability*, 2023, **15**, 16173.
12 K. H. Kucharzyk, R. Darlington, M. Benotti, R. Deeb and E. Hawley, *J. Environ. Manage.*, 2017, **204**, 757–764.
13 S. Deng, Y. Nie, Z. Du, Q. Huang, P. Meng, B. Wang, J. Huang and G. Yu, *J. Hazard. Mater.*, 2015, **282**, 150–157.
14 E. Gagliano, M. Sgroi, P. P. Falciglia, F. G. A. Vagliasindi and P. Roccaro, *Water Res.*, 2020, **171**, 115381.
15 Z. Du, S. Deng, Y. Bei, Q. Huang, B. Wang, J. Huang and G. Yu, *J. Hazard. Mater.*, 2014, **274**, 443–454.
16 S. J. Chow, H. C. Croll, N. Ojeda, J. Klamerus, R. Capelle, J. Oppenheimer, J. G. Jacangelo, K. J. Schwab and C. Prasse, *Water Res.*, 2022, **226**, 119198.
17 F. Dixit, B. Barbeau, S. G. Mostafavi and M. Mohseni, *Environ. Sci.: Water Res. Technol.*, 2019, **5**, 1782–1795.
18 Q. Yu, R. Zhang, S. Deng, J. Huang and G. Yu, *Water Res.*, 2009, **43**, 1150–1158.
19 A. Zaggia, L. Conte, L. Falletti, M. Fant and A. Chiorboli, *Water Res.*, 2016, **91**, 137–146.
20 C. Y. Tang, Q. S. Fu, A. P. Robertson, C. S. Criddle and J. O. Leckie, *Environ. Sci. Technol.*, 2006, **40**, 7343–7349.
21 T. D. Appleman, E. R. V. Dickenson, C. Bellona and C. P. Higgins, *J. Hazard. Mater.*, 2013, **260**, 740–746.
22 J. Heo, L. K. Boateng, J. R. V. Flora, H. Lee, N. Her, Y.-G. Park and Y. Yoon, *J. Membr. Sci.*, 2013, **443**, 69–82.
23 Y. Yoon, P. Westerhoff, S. A. Snyder and E. C. Wert, *J. Membr. Sci.*, 2006, **270**, 88–100.
24 S. Garg, J. Wang, P. Kumar, V. Mishra, H. Arafat, R. S. Sharma and L. F. Dumée, *J. Environ. Chem. Eng.*, 2021, **9**, 105784.
25 F. Fang, S. Chen, K. Shi, S. Xu, Z. Yi, L. Lei, L. Zhuang, H. Wan and Z. Xu, *Sep. Purif. Technol.*, 2024, **348**, 127379.
26 Y. Gao, S. Deng, Z. Du, K. Liu and G. Yu, *J. Hazard. Mater.*, 2017, **323**, 550–557.
27 C. Xu, H. Chen and F. Jiang, *Colloids Surf., A*, 2015, **479**, 60–67.
28 S. Deng, Q. Zhang, Y. Nie, H. Wei, B. Wang, J. Huang, G. Yu and B. Xing, *Environ. Pollut.*, 2012, **168**, 138–144.
29 S. Mantovani, S. Khaliha, L. Favaretto, C. Bettini, A. Bianchi, A. Kovtun, M. Zambianchi, M. Gazzano, B. Casentini, V. Palermo and M. Melucci, *Chem. Commun.*, 2021, **57**, 3765–3768.
30 S. Khaliha, T. D. Marforio, A. Kovtun, S. Mantovani, A. Bianchi, M. Luisa Navacchia, M. Zambianchi, L. Bocchi, N. Boulanger, A. Iakunkov, M. Calvaresi, A. V. Talyzin, V. Palermo and M. Melucci, *FlatChem*, 2021, **29**, 100283.
31 F. Perreault, A. Fonseca de Faria and M. Elimelech, *Chem. Soc. Rev.*, 2015, **44**, 5861–5896.
32 S. Mantovani, S. Khaliha, T. D. Marforio, A. Kovtun, L. Favaretto, F. Tunioli, A. Bianchi, G. Petrone, A. Liscio, V. Palermo, M. Calvaresi, M. L. Navacchia and M. Melucci, *Chem. Commun.*, 2022, **58**, 9766–9769.
33 S. Guo, S. Garaj, A. Bianco and C. Ménard-Moyon, *Nat. Rev. Phys.*, 2022, **4**, 247–262.
34 S. Khaliha, A. Bianchi, A. Kovtun, F. Tunioli, A. Boschi, M. Zambianchi, D. Paci, L. Bocchi, S. Valsecchi, S. Polesello, A. Liscio, M. Bergamini, M. Brunetti, M. Luisa Navacchia, V. Palermo and M. Melucci, *Sep. Purif. Technol.*, 2022, **300**, 121826.

35 **https://www.medica-spa.com/it/news/art/medica-cnr-marchio-graphisulfone**.
36 M. Zambianchi, S. Khaliha, A. Bianchi, F. Tunioli, A. Kovtun, M. L. Navacchia, A. Salatino, Z. Xia, E. Briñas, E. Vázquez, D. Paci, V. Palermo, L. Bocchi, B. Casentini and M. Melucci, *J. Membr. Sci.*, 2022, **658**, 120707.
37 S. Khaliha, F. Tunioli, L. Foti, A. Bianchi, A. Kovtun, T. D. Marforio, M. Zambianchi, C. Bettini, E. Briñas, E. Vázquez, L. Bocchi, V. Palermo, M. Calvaresi, M. L. Navacchia and M. Melucci, *Environ. Sci.: Water Res. Technol.*, 2024, **10**, 1097–1107.
38 F. Tunioli, T. D. Marforio, L. Favaretto, S. Mantovani, A. Pintus, A. Bianchi, A. Kovtun, M. Agnes, V. Palermo, M. Calvaresi, M. L. Navacchia and M. Melucci, *Chem. – Eur. J.*, 2023, **29**, e202301854.
39 I. A. Vacchi, C. Spinato, J. Raya, A. Bianco and C. Ménard-Moyon, *Nanoscale*, 2016, **8**, 13714–13721.
40 K. Spyrou, M. Calvaresi, E. K. Diamanti, T. Tsoufis, D. Gournis, P. Rudolf and F. Zerbetto, *Adv. Funct. Mater.*, 2015, **25**, 263–269.
41 P. Wang, M. Zhang, Y. Lu, J. Meng, Q. Li and X. Lu, *Environ. Int.*, 2019, **129**, 76–85.
42 J. Wang, R. M. Wolf, J. W. Caldwell, P. A. Kollman and D. A. Case, *J. Comput. Chem.*, 2004, **25**, 1157–1174.
43 D. A. Case, R. M. Betz, D. S. Cerutti, T. E. Cheatham III, T. A. Darden, R. E. Duke, T. J. Giese, H. Gohlke, A. W. Goetz, N. Homeyer, S. Izadi, P. Janowski, J. Kaus, A. Kovalenko, T. S. Lee, S. LeGrand, P. Li, C. Lin, T. Luchko, R. Luo, B. Madej, D. Mermelstein, K. M. Merz, G. Monard, H. Nguyen, H. T. Nguyen, I. Omelyan, A. Onufriev, D. R. Roe, A. Roitberg, C. Sagui, C. L. Simmerling, W. M. Botello-Smith, J. Swails, R. C. Walker, J. Wang, R. M. Wolf, X. Wu, L. Xiao and P. A. Kollman, *AMBER*, University of California, San Francisco., 2016.